Quantum calculations of correlated electron-ion collisions in a strong laser field

G. Rascol, H. Bachau, and V. T. Tikhonchuk[a)]
Centre Lasers Intenses et Applications, UMR 5107, Université Bordeaux 1-CNRS-CEA, 33405 Talence Cedex, France

H.-J. Kull and T. Ristow
Institute of Theoretical Physics A, Rheinisch Westfälische Technische Hochschule, D-52056 Aachen, Germany

(Received 17 August 2006; accepted 7 September 2006; published online 31 October 2006)

The energy spectrum and angular distribution of electrons scattered by an ion in a strong laser field are investigated as a function of the incident electron velocity for small impact parameters. The energy distribution has been calculated quantum-mechanically by a method of wave-packet scattering from a three-dimensional hydrogen-like Coulomb potential. It is compared with the energy distribution from the classical instantaneous collision model, and the quantum limitations are evaluated. The backscattered particles can have enhanced scattering rates and a very large energy gain due to the effect of correlated collisions. Their spectrum displays a ring structure similar to the rescattering plateau in the above-threshold ionization of neutral atoms. The effect of these large-angle scattering effects on the electron acceleration and heating is also discussed.
 [DOI: 10.1063/1.2358968]

I. INTRODUCTION

Electron-ion collisions in plasmas are usually considered in the Born approximation by assuming a small deviation of the electron orbit in the Coulomb field of the ion. The large-angle scattering events are often neglected because of the long-range nature of electrostatic interaction. The interactions at large impact parameters dominate and have a cutoff at the Debye screening length. A similar approach is widely used for electron-ion collisions in a high-frequency laser field. The effective Rutherford cross section and the cutoff at large impact parameters were modified by taking into account the electron quiver velocity in the laser field.[1,2] The classical approach to electron-ion collisions was later confirmed by quantum-mechanical calculations.[3–5] More recent publications[6–10] have essentially confirmed the original results with certain improvements for strong laser fields and for strongly coupled plasmas.

The effect of small impact parameters and correlated collisions due to the Coulomb focusing in a high-frequency electric field was brought to attention in Ref. 11 and considered in more detail in Ref. 12. By solving the dynamic equation for the electron orbits in the combined laser and Coulomb field, it was found that for certain phases and impact parameters the electron exhibits a chaotic motion and sometimes gains a large energy. This effect arises due to multiple, correlated collisions and might lead to abnormally large heating rates.[12,13] It has also been shown to play an important role in laser pulse interaction with clusters.[14] However, validity of the classical approach is not evident because the correlation effects come into play for impact parameters much smaller than the Bohr radius where the quantum effects might be important. In spite of the well-known similarity between the classical and quantum description of electron-ion Coulomb collisions, it is not evident that this similarity is maintained if the high-frequency electric field is added.

The quantum effects in laser-assisted electron-ion collisions were considered in Ref. 15. It was shown that large-angle collisions form a high-energy tail in the electron energy distribution and that the effect of correlated collisions of free electrons is very similar to the effect of above-threshold ionization of neutral atoms,[16] especially if the velocity of the incoming electron is of the order of the atomic velocity. Rescattering of a newly ionized electron is of the same nature as a collision of a free electron with a small impact parameter. The quantum calculations show an extended plateau in the energy spectrum of backscattered electrons modulated by the photon energy of the laser.

However, the one-dimensional quantum-mechanical calculations employed in Ref. 15 cannot address the question of the minimum impact parameter because the real Coulomb potential is artificially smoothed near the origin. Only realistic three-dimensional solutions to the Schrödinger equation can address this problem. This is the main objective of the present paper—to carry out the numerical solutions to the time-dependent Schrödinger equation and to compare them with the one-dimensional quantum results obtained previously and with the classical dynamical model and the model of instantaneous collisions.[4,9,15]

The paper is organized as follows. The quantum-mechanical and classical models are presented in Sec. II. We discuss the basic assumptions and numerical implementations. The results from the numerical simulations and their analysis are presented in Sec. III. Because of certain computing limitations, we limit ourselves to relatively slow electrons with energies of tens of eV, which are most susceptible

[a)]Electronic mail: tikhon@celia.u-bordeaux1.fr

to the correlation effects and to relatively short laser pulses of the order of a few periods. However, by comparing the quantum and classical results, we will show how the results could be extended to a broader parameter domain. We will discuss the manifestations of the correlation effects in the angular distribution and the energy spectrum of scattered electrons, and we will show that no special cutoff is needed at small impact parameters. Section IV presents our concluding remarks.

II. PRESENTATION OF THE MODELS

A. Time-dependent Schrödinger equation: The spectral method

The electron motion has been described by the time-dependent Schrödinger equation (TDSE),

$$i\partial_t \Psi(\boldsymbol{r},t) = \left[-\frac{1}{2}\nabla^2 - \frac{Z}{r} - i\boldsymbol{A}(t)\cdot\nabla \right]\Psi(\boldsymbol{r},t) \tag{1}$$

for the electron wave function $\Psi(\boldsymbol{r},t)$ with the Hamiltonian, which is a sum of the Hamiltonian of the hydrogenic atom, $H_0=\boldsymbol{k}^2/2-Z/r$, and the interaction with the laser field, $\boldsymbol{A}(t)\cdot\boldsymbol{k}$, depending explicitly on time. The ion of a charge Z is at the origin and $\boldsymbol{k}=-i\nabla$ is the momentum operator. From now on, all formulas are presented in atomic units, that is, the length is measured in units of the Bohr radius, $a_B=\hbar^2/e^2m_e$, the momentum in $m_e e^2/\hbar$, and the energy in e^2/a_B. The interaction term was calculated in the velocity gauge; the vector $\boldsymbol{A}$ is directed along the z axis and it varies over time with the frequency ω in the time interval $(-\tau/2,\tau/2)$ as

$$A_z(t) = -\frac{\mathcal{E}_0}{\omega_0}\cos^2\left(\frac{\pi t}{\tau}\right)\sin(\omega_0 t+\phi), \tag{2}$$

where $\mathcal{E}_0$ is the amplitude of the electric field, ω_0 is its frequency, and τ is the total pulse duration. Considering nonrelativistic particles, we neglect the effects of magnetic fields and the spatial variation of the electric field.

Equation (1) has been solved by the spectral method, which is extensively used in atomic physics and the theory of strong fields.[17] It is employed here in the context of L2 functions and the B-splines. (See Ref. 18 for a review of the applications of B-splines in atomic and molecular physics.) The equation is solved in spherical coordinates with the z axis along the electric field polarization (2). We restrict ourselves to the particular case of a parallel launch where the packet of electrons was sent along the z axis, parallel to the electric field vector, therefore the azimuthal number is set to $m=0$. It is known from previous studies[13] that the correlation effects are more important in this case.

We consider a wave packet that is initially at $t=-\tau/2$ centered around a certain position $z_0=-r_0$ on the z axis and then moving in the positive z direction. The initial condition to Eq. (1) corresponds to the incident wave packet

$$\Psi_0(\boldsymbol{r}) = \Psi(r,\theta,-\tau/2) = N^{-1/2}\Psi_\perp e^{ik_0 z-(r-r_0)^2/d_0^2}, \tag{3}$$

where N is a normalization factor and $\Psi_\perp$ defines the angular distribution of the incident packet,

$$\Psi_\perp = \begin{cases} 0, & 0\le\theta\le\theta_{\max}, \\ \cos^4[\pi(\pi-\theta)/2(\pi-\theta_{\max})], & \theta_{\max}\le\theta<\pi. \end{cases} \tag{4}$$

The position r_0 at $t=-\tau/2$, the spatial width, d_0, the angular width, $\theta_{\max}$, and the initial velocity, k_0, were chosen in such a manner that the wave-packet maximum is supposed to pass the origin at the time of the maximum of the envelope of the electric field, $t\approx 0$. To resolve multiphoton energy spectra, the width d_0 of the wave packet has to be chosen large enough such that the energy width $\Delta E=k_0\Delta k$ is smaller than the photon energy ω_0. Using the momentum width $\Delta k=1/d_0$ yields the requirement $d_0\gg k_0/\omega_0$. This is also the condition for complete averaging over the phases of the laser field within the width of the wave packet. The typical parameters for the calculations presented below are: $k_0=0.7$, $r_0=44$, $d_0=17$, and $\theta_{\max}=2.37$ rad.

The solution of the TDSE (1) is expanded in a series, $\Psi(\boldsymbol{r},t)=\Sigma_{n,l}C_{n,l}(t)\Phi_{n,l}(\boldsymbol{r})$ for $n\le n_{\max}$ and $l\le l_{\max}$, and the temporal evolution of the coefficients $C_{n,l}$ has been calculated. The basis wave functions $\Phi_{n,l}$ are eigenstates of the free atom Hamiltonian H_0. They are expanded in spherical harmonics Y_l^m as follows:

$$\Phi_{n,l}(\boldsymbol{r}) = \sum_{i=1,i_{\max}} c_i B_i^q(r) Y_l^0(\theta). \tag{5}$$

The coefficients c_i are determined by using a diagonalization procedure, which leads to the determination of the eigenvectors $\Phi_{n,l}$ and associated eigenenergies $E_{n,l}$. The lowest (negative) energies represent the bound states while the positive energies are associated with the discretized continuum. The B-spline functions $B_i^q(r)$ represent the radial part of the wave functions. They are of the order $q=6$ and are defined, in our case, on a linear knot sequence.[19] B-splines are confined in a radial box of a length $R_{\max}$.

The general procedure followed here to determine $\Psi(\boldsymbol{r},t)=\Sigma_{n,l}C_{n,l}(t)\Phi_{n,l}(\boldsymbol{r})$ is similar to the one previously used in the context of multiphoton ionization.[17] The main difference is that the initial state is not the fundamental orbital of the atom, but the incident wave packet (3). Equation (1) is integrated over the total pulse duration τ with the initial condition

$$C_{n,l}(-\tau/2) = \langle \Phi_{n,l}(\boldsymbol{r})|\Psi_0(\boldsymbol{r})\rangle. \tag{6}$$

A Runge-Kutta method is used for the time integration of $C_{n,l}(t)$ in the interaction representation of Eq. (1).

The number of angular momenta $l_{\max}\simeq 40$, the number of eigenstates $n_{\max}\simeq 350$, and the number of B-splines $i_{\max}\simeq 400$ were chosen from conditions for the numerical convergence, precision, and performance. The box length $R_{\max}\simeq 250$ was chosen in such a manner that the wave function does not reach the limit of the box at the end of the run. These conditions impose certain limits on the total pulse duration and initial velocity.

Having obtained the solution at $t=\tau/2$, the population of the energy states is given by $|C_{n,l}(\tau/2)|^2$. It gives a direct access to the energy spectrum $p(E)$. Another important quantity is the momentum distribution at the end of the pulse, which is the Fourier transform of the wave function at the final time,

$$\psi(\boldsymbol{k}) = \mathrm{FT}_{\boldsymbol{r}}\Psi(\boldsymbol{r}, t=\tau/2). \tag{7}$$

In order to compare the present results with previous one-dimensional simulations,[15] we also calculated a partial Fourier transform of the wave function along the propagation direction, $\psi_1(k_z)=\mathrm{FT}_z\Psi(x=0,y=0,z,t=\tau/2)$, and the distribution of momenta in this direction, $\psi_2(k_z)=\mathrm{FT}_r\psi(k_x=0,k_y=0,k_z)$.

B. Time-dependent Schrödinger equation: The grid method

The spectral method of solution to the TDSE equation allows one to obtain very fine resolution near the scattering center and therefore to explore rather small impact parameters with high precision. However, it is limited to the volumes of a few hundred atomic units, which makes access to high impact velocities and long pulse durations difficult. The grid method offers a possibility to explore these limits.

The TDSE is solved in cylindrical coordinates by a two-dimensional alternating-direction implicit (ADI) finite-difference scheme.[20] The scattering problem with parallel launch has cylindrical symmetry and it is therefore sufficient to calculate cylindrically symmetric solutions of the two cylindrical coordinates z and ϱ. Equation (1) is written in the Kramers-Henneberger frame, using a coordinate system whose origin is moving with the quiver motion of a free electron in the laser field. The ion is oscillating about the origin with the electron quiver amplitude in the laser field (2): $\mathcal{E}_z(t)=-\partial_t A_z$. Correspondingly, the velocity of the oscillation frame is given by $v_{z,KH}=A_z$ and the coordinate by $z_{\mathrm{KH}}(t)=\int dt A_z(t)$.

The initial wave function $\Psi_0(r,\varrho)$ is of a similar form to that of Eq. (3),

$$\psi_0(\varrho,z) = \left(\sqrt{\frac{2}{\pi}}\frac{1}{d_0}\right)^{3/2}\psi_\perp(\varrho)\mathrm{e}^{ik_0 z-(z-z_0)^2/d_0^2}. \tag{8}$$

The main difference from Sec. II A is that the function $\Psi_\perp$ was chosen as a Gaussian

$$\Psi_\perp = \mathrm{e}^{-\varrho^2/\varrho_0^2} \tag{9}$$

with the same width $\varrho_0=d_0$ as in the axial direction. In the present calculations, we have chosen $z_0=-k_0\tau/2$ and the grid boundaries are at $z_{\max}=\pm 350$ and $\varrho_{\max}=350$ to avoid wave-function reflections back into the computational volume.

The packet radius ϱ_0 was chosen in such a way that the wave functions (4) and (9) were normalized similarly,

$$\int |\psi_\perp|^2 d^2\varrho = \frac{\pi}{2}\varrho_0^2. \tag{10}$$

That gives a relation between ϱ_0 in Eq. (9) and $\theta_{\max}$ in Eq. (4), $\varrho_0=0.43r_0(\pi-\theta_{\max})$. Then the functions (4) and (9) differ less than 4% in the domain of interest.

The energy distribution is calculated at the end of the run at $\tau/2$ by a spatial Fourier transformation (7). The momentum probability distribution $p(\boldsymbol{k})=|\psi(\boldsymbol{k})|^2$ is normalized to unity in the momentum space as the wave function is normalized to unity in the coordinate space. The energy distribution of the kinetic energy operator $\boldsymbol{k}^2/2$ is obtained from the momentum distribution according to

$$p(E) = \langle\psi|\delta(\boldsymbol{k}^2/2-E)|\psi\rangle. \tag{11}$$

For simplicity, we do not calculate the spectrum of the total energy since the scattered particles belong mostly to continuum states, although the bound states also contribute to this energy distribution. For instance, calculating the kinetic energy distribution (11) with the ground-state wave function $\psi_0=e^{-r}/\sqrt{\pi}$ of hydrogen yields

$$p(E) = \frac{32}{\pi}\frac{\sqrt{2E}}{(1+2E)^4}.$$

In practice, the bound-state contribution can be clearly distinguished from the free-electron contribution since it is not or only weakly modulated by multiphoton peaks. The bound-state contribution governs the asymptotic behavior of the high-energy tail beyond the cutoff for multiphoton absorption [see Eq. (15)]. As an example, the energy distribution for the initial wave packet (8) is given by

$$p(E) = \sqrt{\frac{2}{\pi}}\frac{d_0}{k_0}\mathrm{e}^{-d_0^2(E+k_0^2/2)}\sinh(k_0 d_0^2\sqrt{2E}). \tag{12}$$

It corresponds to a narrow maximum at the incident electron energy $E_0=k_0^2/2$ with the width corresponding to the effective temperature $T_{eff}=1/d_0^2$.

Both methods of the numerical solution to the TDSE were verified with the exact solution for the case of the electron-ion scattering without external fields and for mutual consistency.

C. Model of classical collisions

The results of quantum-mechanical calculations are compared to a dynamical model,[12,13] which calculates classical electron orbits in the combined ion potential and the oscillating electric field with

$$\frac{d\boldsymbol{r}}{dt} = \boldsymbol{v}, \quad \frac{d\boldsymbol{v}}{dt} = -\frac{Z\boldsymbol{r}}{(r^2+\varepsilon^2)^{3/2}} - \mathcal{E}(t), \tag{13}$$

where the electric field has only a z component, $\mathcal{E}_z=-\partial_t A_z$. The parameter ε serves two purposes: first, it stabilizes the numerical solution to Eqs. (13); second, it models a small-distance cutoff such as the de Broglie length $1/k_0$, which may be needed to account for quantum effects. In contrast to a simplified model of instantaneous collisions that was developed in Refs. 4 and 9 for small-angle scattering, this dynamical model could be applied for the interaction at small impact parameters and can account for the rescattering effect.

The system (13) was numerically solved for a certain number of initial conditions. Furthermore, the energy spectrum of electrons was evaluated by averaging over the initial positions. As the electric field is polarized in the axial direction, parallel to the initial velocity, all electron orbits lay in the plane of incidence and the cylindrical geometry was accounted for by an appropriate weighting.

In order to make an appropriate comparison between the quantum and classical models, the initial distribution of the electrons in the classical calculations should be chosen in a way to model as closely as possible the quantum electron distribution function. Therefore, the distribution of the particles has to be chosen according to Eq. (3), $f_0(\boldsymbol{r})=|\Psi_0(\boldsymbol{r})|^2$. However, it is not exactly so. In fact, the classical distribution has to be taken with a larger width considering the quantum dispersion of the wave packet on its way from the starting point to the scattering center.[15]

In order to account for this effect in the classical model, let us recall that the Gaussian distribution function (3) and (9) in free space conserves its shape, while the maximum is displaced as $z_m(t)=z_0+k_0(t+\tau/2)$ and the width increases as $d(t)=\sqrt{d_0^2+4(t+\tau/2)^2/d_0^2}$. [The diffraction is more complicated in radial direction for function (4), but qualitatively the radial width follows the same dependence as $d(t)$.] Assuming that the initial distance z_0 is given, one has to choose the initial dispersion in such a way that the dispersion at $t=0$ would be as small as possible, that is, $d_0=|2z_0/k_0|^{1/2}$. This corresponds to a minimum spread of the initial wave packet before the interaction, which is of the order of 40%. Moreover, in the classical model, the initial width should be taken larger, $d_c=d_0\sqrt{2}$, to account for the quantum dispersion at the moment of collision. In the simulations presented in the next section, the initial velocities were varied in the range $0.4<k_0<3$ and the initial distance (dictated by the laser pulse duration, $\omega_0\tau/2\pi\sim 4-6$) was $|z_0|\sim k_0\tau/2$, and therefore the initial width was $d_0\sim\sqrt{\tau}$.

The motivation for the choice of the radial packet width (10) is related to the maximum impact parameter for the scattering process. It is well known that the Rutherford cross section diverges at large impact parameters. However, the external oscillating electric field eliminates this divergence and cuts off the Coulomb interaction at the distances $\sim k_0/\omega_0$. This follows straightforwardly from the solution of the classical model (13) in the Born approximation. For this reason, the initial radial width of the wave packet was chosen, $\varrho_0>(3-6)k_0/\omega_0$, and it was verified that the choice $\varrho_0=r_0$ satisfies this criterion. The initial radial width in the classical simulations, $\varrho_c=\sqrt{\varrho_0^2+4z_0^2/k_0^2\varrho_0^2}\sim\sqrt{2}d_0$, accounts for the radial dispersion.

III. ELECTRON ENERGY SPECTRUM

The energy spectrum is determined by primary scattering and by a number of secondary processes, including rescattering, recombination, and ionization. In the study of ATI, it was recognized that the ionization is accompanied by scattering of ionized electrons. Conversely, the scattering is accompanied to some extend by the ATI of recombined electrons. Furthermore, the classical effect of correlated collisions will also enhance the quantum-mechanical scattering rates. To distinguish between these processes in more detail, we have compared scattering from an attractive ($Z=+1$) and a repulsive ($Z=-1$) potential. Since a repulsive potential has no bound states and deflects the electron away from the scattering center, subsequent interactions with the ion will be negligible. The repulsive case is therefore taken as a reference for the pure scattering process as described, e.g., by the instantaneous collision model. On the other hand, attractive potentials will allow for a number of correlation effects that ultimately lead to enhanced scattering rates.

It is also instructive to consider the origin of correlated collisions from the quantum-mechanical viewpoint. In quantum mechanics, the concept of electron orbits loses its validity, however the classical focusing of the electron orbits by an attractive potential corresponds to an increased spatial probability density in the region behind the scattering center. Actually the scattering amplitude for Coulomb scattering is basically proportional to Z. As a result, the outgoing scattering wave interferes differently with the incoming wave depending on the sign of Z. In the forward direction, one obtains an interference maximum for an attractive and an interference minimum for a repulsive potential. Subsequent laser-driven collisions are thereby enhanced in the attractive case.

A. Effect of initial parameters

The set of parameters chosen for the simulations presented above is the following: the ion charge $Z=1$, the laser frequency $\omega_0=0.3$ (corresponding to a wavelength of 150 nm, the energy $\hbar\omega_0=8.2$ eV, and the period of 0.5 fs), the electric field $\mathcal{E}_0=0.3$ (the corresponding intensity 3.16×10^{15} W/cm^2), the pulse duration four to six periods, that is, 2–3 fs, and the electron velocity $k_0=0.7$ (the energy of 13.5 eV). Such parameters can be achieved by the present-day free-electron lasers.[21] The ponderomotive potential for these parameters $U_p=(\mathcal{E}_0/2\omega_0)^2$ is comparable to the photon energy ω_0 and multiphoton processes are therefore expected. A dimensionless measure for the strength of the field is the strong field parameter Ω introduced in Ref. 12. It can be expressed as the ratio of the characteristic value of the electrostatic potential, Z/ξ_0, to the kinetic energy of an oscillating electron,

$$\Omega=(Z/\xi_0 v_0^2)^{1/4}=Z^{1/4}\omega_0/\mathcal{E}_0^{3/4}, \tag{14}$$

where $\xi_0=v_0/\omega_0$ and $v_0=\mathcal{E}_0/\omega_0$ are the electron quiver radius and the quiver velocity. For $\Omega<1$, correlation effects in strong laser fields have been demonstrated in the classical treatment.[12]

Corresponding to the discussion in the previous section, the packet launch distance was $z_0=-44$ and the dispersion $d_0=17$. Figure 1 shows the comparison of energy spectra $p(E)$ of scattered particles obtained with the quantum and classical models. The parameters of the initial distribution in the classical model were chosen according to the prescriptions of Sec. II C.

One can see that both numerical methods produce rather similar energy distributions [solid and dotted curves in panels (a) and (b)], although the methods of calculation of the probability function are different. In the spectral method, $p(E)$ is represented as a sum of populations of the hydrogen eigenstates, while in the ADI method this is the momentum probability distribution weighted by the kinetic energy and integrated over the energy shells (11). The electron energy distribution consists of three distinct elements: (i) a peak at

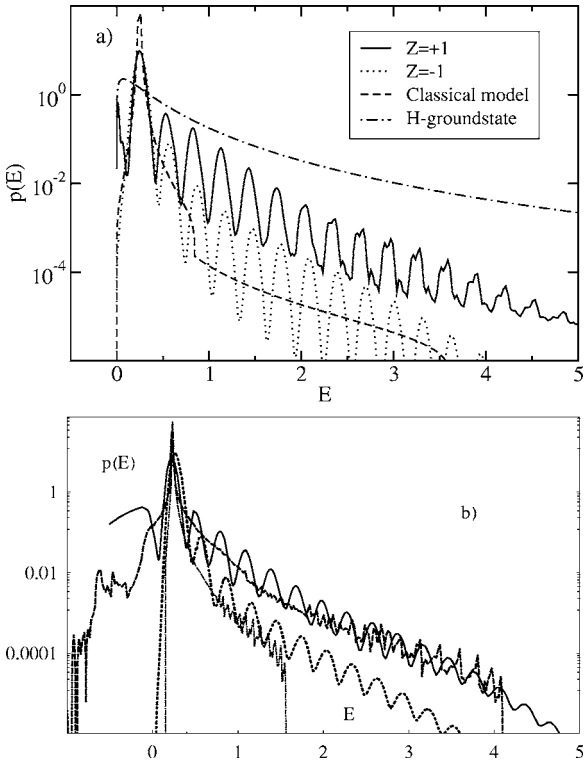

FIG. 1. Electron energy spectra obtained from the quantum and classical models for the following set of parameters: $k_0=0.7$, $\mathcal{E}_0=0.3$, $\omega_0=0.3$, $\tau=125$. (a) Spectrum obtained with the ADI method for $Z=1$ (solid line) and $Z=-1$ (dotted line); (b) the same spectrum obtained with the spectral method for $Z=1$ (solid line) and $Z=-1$ (dotted line). The thick dashed (thin dash-dotted) line in panel (b) shows the result of the classical dynamical model for $Z=1$ ($Z=-1$). The dashed line in panel (a) shows the result of the classical model of instantaneous collisions. Also shown for comparison is the energy spectrum of the electron in the ground state of hydrogen (dotted-dashed line).

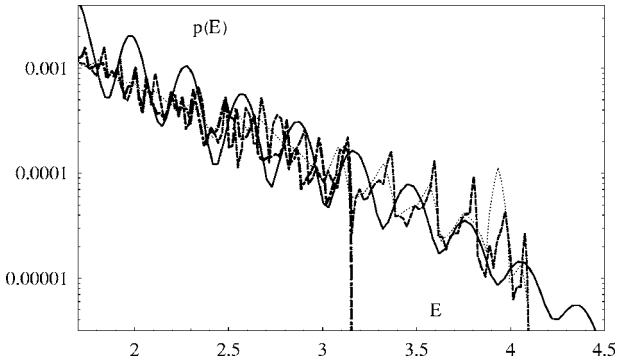

FIG. 2. Influence of the parameter $\varepsilon=10^{-2}$ (thick dash-dotted line), 10^{-4} (thick dashed line), and 10^{-6} (thin dotted line) on the cutoff energy in classical model simulations. The solid curve presents the distribution obtained from the quantum calculation. The parameters are the same as in Fig. 1.

the incident energy $E_0=\frac{1}{2}k_0^2=0.25$ broadened due to the dispersion; (ii) a tail (or a plateau) modulated with the photon energy ω_0, and (iii) a certain number of trapped particles, corresponding to negative energies.

For comparison, we show in Fig. 1(a) the energy spectrum of scattered electrons calculated within the model of instantaneous collision.[15] This model was proposed long ago,[4,9] and it supposes that the role of the laser field is reduced to a kick to the electron drift velocity k_0 at the moment of collision. The classical curve corresponding to the instantaneous collision model follows rather well the quantum solution with $Z=-1$ with the sharp cutoff at the energy 3.65. It corresponds to the maximum energy gain in a head-on collision. Indeed, since the collision time $\tau_{coll}\sim 1/k$ is much shorter than the laser period, the role of the laser field is actually reduced to spread the incident electron velocity k_0 into the range (k_0-v_0,k_0+v_0), depending on the phase of the electric field. The fastest moving electrons after the head-on collision will have the velocity $-k_0-v_0$, that is, $-k_0-2v_0$ as a drift velocity. This consideration predicts the cutoff energy,

$$E_{\max}=\tfrac{1}{2}(k_0+2v_0)^2. \tag{15}$$

The classical dynamical model described in Sec. II C agrees qualitatively with that analysis for relatively high electron energies, where the Coulomb potential energy can be neglected at the reflection point. However, for slow electrons, $k_0<1$, the latter effect leads to a higher cutoff for the attractive potential, $Z=1$, and to lower cutoff for the repulsive one, $Z=-1$. This effect is visible in Fig. 1(b). The high-energy cutoff is much less visible in quantum curves, but their slopes become steeper at this energy.

In the case of a positive ion, the spectrum is more complicated. The additional recombination-ionization and rescattering processes lead to a largely enhanced fast electron spectrum. In the ADI calculation, the slope of the high-energy tail agrees with the asymptotic power law $\propto E^{-3.5}$ corresponding to the kinetic energy distribution of the hydrogen ground state shown by the dotted-dashed line in panel (a). This is another indication of correlation effects. The ratio between the asymptotic electron distribution function $p(E)$ for $E\gtrsim 5$, $Z=1$ and that for the hydrogen ground state gives an estimate of the population of bound states in the scattered electron spectrum.

The pure scattering spectrum cannot exclusively be recognized in this case because of its steeper slope in the high-energy tail. Nevertheless, in contrast to the instantaneous collision model, the classical dynamical model agrees rather well with the quantum calculations, as can be seen in panel (b).

The appropriate choice of the widths of the classical distribution, d_c and ρ_c, is rather important for this agreement. By decreasing the widths in the classical model, one would strongly overestimate the number of fast particles and their effective temperature. It was also verified that the spectrum of scattered electrons is rather insensitive to the pulse duration, which was verified in calculations with pulses of four and six laser periods. However, the classical model predicts more trapped particles with negative energies, partially even below the ground-state energy. This is an evident contradiction with the laws of quantum mechanics. The lowest level of the hydrogen atom corresponds to $E=-0.5$, which is the low-energy cutoff in the quantum curves. However, the trapping probability is rather small, less than 10^{-3} for the present parameters.

Another important parameter in the classical calculations is the minimal distance ε in Eqs. (13). Figure 2 shows the

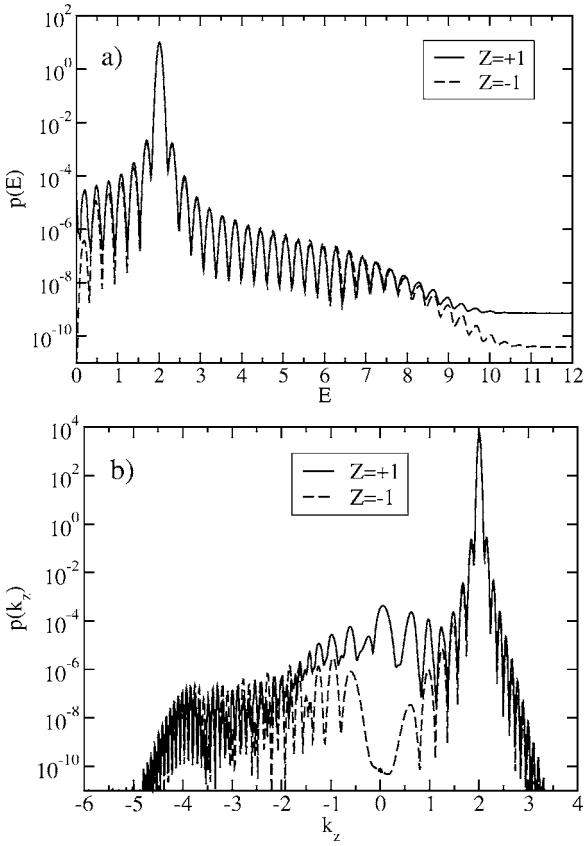

FIG. 3. Energy spectrum $p(E)$ (11) (a) and momentum spectrum $p(k_z)=|\psi_2(k_z)|^2$ (b) of scattered electrons for the incident velocity $k_0=2$, for $Z=1$ (solid line) and $Z=-1$ (dashed line). Other parameters are the same as in Fig. 1. The TDSE is solved with the ADI method.

effect of this parameter on the classical energy spectrum for the same physical parameters as in the previous figures. Choosing $\varepsilon > 10^{-4}$, the cutoff energy is significantly reduced, while smaller values have no apparent influence, although the calculations with larger ε are preferred due to numerical reasons. The best agreement with the quantum results was always obtained for the smallest ε, usually less than 10^{-4}. This observation leads us to two conclusions. First, the classical model with no minimum cutoff parameter can be considered as the best approximation of the quantum model. This confirms the correctness of the classical model used in the previous studies[12,13] and indicates that electrons can approach the nuclei up to distances two to three orders of magnitude smaller than the atomic radius. Second, in the numerical calculations with the classical model, the appropriate value of the cutoff parameter should be chosen in such a way that it does not affect the final results.

The effect of correlated collisions strongly depends on the velocity of the incident electron. This can be concluded by comparing the scattering spectra for positive and negative ions. The energy spectra for $k_0=2$ shown in Fig. 3 are very close to each other and therefore the instantaneous collision model produces more adequate results. The criterion for that is $k_0 \gg v_0$, so the electron will never return to the ion.

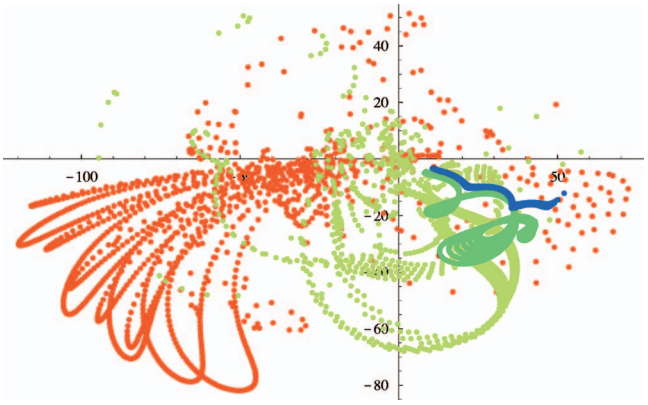

FIG. 4. (Color) Position of particles at the end of classical calculations sent within the certain range of impact parameters: red, $0<\varrho<1$; yellow, $2<\varrho<2.4$; green, $6.5<\varrho<7.3$; blue, $10<\varrho<12$. The parameters are the same as in Fig. 1.

IV. ANGULAR DISTRIBUTION OF SCATTERED ELECTRONS

The classical analysis suggests that the electrons that acquire the maximum energy are scattered in the backward direction and therefore approach the ion with small impact parameters. Figure 4 shows the final positions of the particles sent at various impact parameters. Indeed, only the particles incident at small impact parameters are scattered in the backward direction. They also exhibit a chaotic behavior: due to the correlation effect, they could be scattered in any direction and the final position is not a smooth function of the initial parameters. On the contrary, the particles with large impact parameters, $\varrho > 10$, exhibit a completely regular motion, scattered only in small angles, and do not gain much energy—their final positions are compact and at a relatively small distance from the center.

Quantum calculations essentially confirm these observations. The momentum spectra of particles scattered backward and forward have been calculated by Eq. (7). The distribution $|\psi_1(k_z)|^2$, shown in Fig. 5, has been obtained by the spectral method. The calculation by the grid method gives a similar result. Two complementary effects—the head-on instantaneous collisions and the recombination-ionization process—can be clearly identified. The distribution is strongly asymmetric: only the part of negative k_z exhibits a plateau with the cutoff velocity defined by Eq. (15). In addition, the difference between $Z=1$ and -1 due to the bound states is evident. The slope of the particle distribution for the positive scattering center corresponds to the asymptotic of the bounded state. This is in agreement with the previous discussion concerning Fig. 1(a).

The plateau formation becomes even more evident for higher incident energies, in spite of the fact that the total number of energetic particles decreases. Figure 3(b) shows the momentum distributions $|\psi_2(k_z)|^2$ for the case $k_0=2$ for the positive and negative scattering centers. The plateau is the same for both cases, while the trapped electrons are clearly present in the positive charge case.

Figure 6 shows complete spatial and momentum distributions for $k_0=2$. The energetic particles have a rather broad

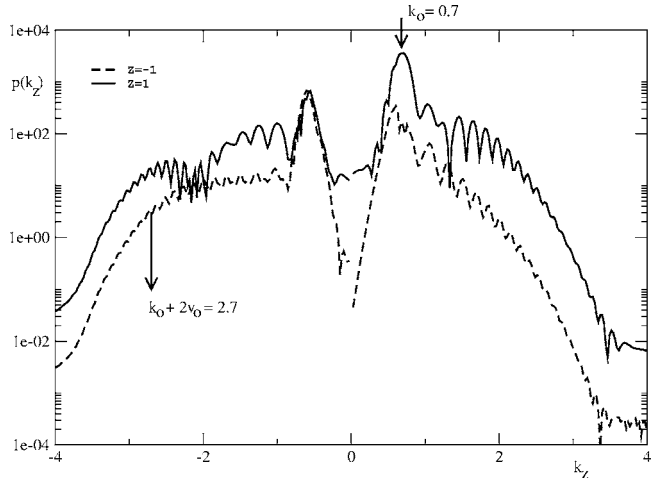

FIG. 5. Momentum distribution of scattered particles in the propagation direction $p(k_z)=|\psi_1(k_z)|^2$ for the quantum calculations for $Z=1$ (solid line) and $Z=-1$ (dashed line). The parameters are the same as in Fig. 1. The TDSE is solved with the spectral method.

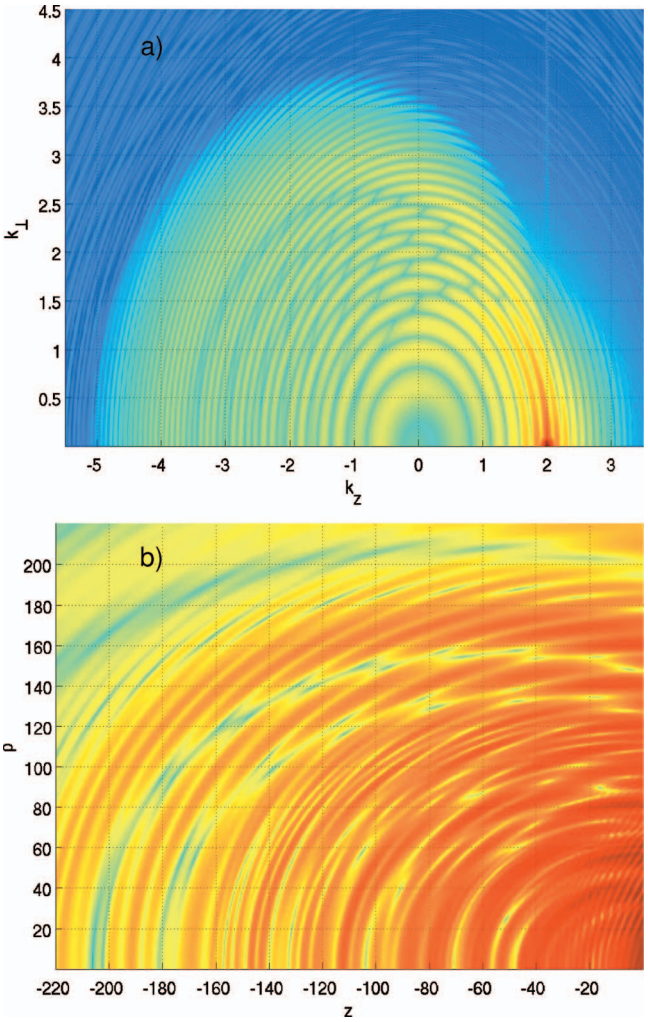

FIG. 6. (Color) Probability density distributions of (a) momentum and (b) position of the scattered particle for the incident velocity $k_0=2$. Probability decreases on a logarithmic scale from red to blue. The potential is repulsive ($Z=-1$) and other parameters are the same as in Fig. 1. The TDSE is solved with the ADI method.

angular spectrum. The multiphoton effect manifests itself in the spherical shell structure of the distributions. The momentum distribution is in good agreement with the classically allowed region $\boldsymbol{k}=\boldsymbol{p}-A_z\boldsymbol{e}_z$ determined by the quiver momentum with amplitude $A_z=E_0/\omega_0=1$ and the impact momentum $\boldsymbol{p}$ with magnitude $p=k_0+A_z=3$. It describes a circle in the $\boldsymbol{k}$ plane around the center $(k_z=-1, k_\perp=0)$ with the radius $p=3$. Note that this circle is not concentric with the energy shells around the origin. Therefore, one passes different maxima and minima in going on a given energy shell around the scattering center. These maxima, rotated around the polarization direction, produce the scattering rings observed under similar conditions in ATI experiments.[22] The spatial distribution shows basically the same features since the positions of the density maxima of the outer shells are determined by free propagation.

Using the formula for the scattering angle in the Coulomb field, $\cot(\theta/2)=k_0^2\varrho/Z$, one can estimate the range of impact parameters, $\varrho\lesssim 2$, which would contribute to this large-angle scattering in the case without laser field. An increase of the backscattering indicates the importance of the effect of correlated collisions. As it was explained in Refs. 12 and 13, the electron with larger impact parameters experiences *Coulomb focusing*; it could be attracted toward the ion and scattered eventually to a large angle. This was also called the *parachute effect* in Ref. 12. The characteristic impact parameter for the correlated collision, $\varrho_{corr}\approx\sqrt{Z/\mathcal{E}_0}\sim 2$, can be estimated as follows. A relatively slow electron, $k_0<v_0$, with an impact parameter ϱ is deviated to the angle $\delta\theta\sim 2Z/v_0^2\varrho$ while passing the ion. That means the electron acquires a perpendicular velocity $v_\perp\sim v_0\delta\theta$ and it can arrive in a head-on collision with the ion after half a laser period if $\varrho=\pi v_\perp/\omega_0$. One may expect multiple returns if the electron is very slow, $k_0\ll v_0$. Although for our choice of parameters multiple returns are not important, the correlated collisions indeed increase the number of backscattered electrons. In fact, they create a population of fast electrons, which could be important for certain secondary effects like ionization, line emission, etc. As was shown in Ref. 23, this effect can be further enhanced in the case of high-Z ions, because the effective cross section of the correlated collisions, $\sim\varrho_{corr}^2$, increases with the ion charge.

V. AVERAGE CHARACTERISTICS OF THE ACCELERATED ELECTRONS

Having defined the correspondence between the quantum and classical models, we discuss now the parametric dependencies of the effect of electron acceleration. The parameters that we analyze are as follows. (i) The maximum energy of accelerated electrons, $E_{\max}$ [the classical estimate is given by Eq. (15)]. (ii) The probability for the electron to gain an energy $E>E_c$, $n_h=\int_{E_c}^{E_{\max}}p(E)dE$. Following Ref. 15, we introduced an empirical threshold E_c related to the ponderomotive potential, $U_p=\mathcal{E}_0^2/4\omega_0^2$, and consider a particle to belong to the hot population if its energy gain exceeds three ponderomotive potentials, $E_c=\frac{1}{2}k_0^2+3U_p$. (iii) The mean en-

TABLE I. Characteristic parameters of the calculations and the accelerated electrons for the electron scattering on the attractive $Z=1$ and repulsive $Z=-1$ charge; a comparison between the quantum-mechanical (qm) and classical (cl) calculations and the theoretical (th) formula (15).

k_0	$\mathcal{E}_0$	ω_0	v_0	Z	Ω	E_c	$E_{\max}$ qm	$E_{\max}$ cl	$E_{\max}$ th	E_h qm	E_h cl	n_h% qm	n_h% cl
0.4	0.2	0.3	0.66	1	1.0	0.413	2.5	2.0	1.5	0.71	0.6	3.3	3.0
0.7	0.2	0.3	0.66	1	1.0	0.58	3.0	2.4	2.1	0.84	0.79	1.1	0.93
0.7	0.3	0.3	1.0	1	0.74	0.995	4.5	4.1	3.65	1.36	1.41	0.95	0.36
0.7	0.3	0.3	1.0	−1	0.74	0.995	4.6	1.6	3.65	1.36	1.17	0.047	0.016
1	0.3	0.3	1.0	1	0.74	1.25	5.0	4.74	4.5	1.68	1.79	0.10	0.14
1.5	0.2	0.3	0.66	1	1.0	1.45	4.0	4.0	4.0	1.61	1.87	0.02	0.075
1.5	0.3	0.3	1.0	1	0.74	1.87	6.5	6.3	6.1	2.49	2.61	0.002	0.053
2.0	0.3	0.3	1.0	1	0.74	2.75	8.0	8.1	8.0	3.43	3.66	0.00035	0.032
2.0	0.3	0.3	1.0	−1	0.74	2.75	8.0	7.8	8.0	3.8	3.66	0.00034	0.030

ergy of accelerated particles, $E_h=n_h^{-1}\int_{E_c}^{E_{\max}}Ep(E)dE$. Some results concerning the parameters of hot electrons are presented in Table I.

One can see that there is quite a reasonable general agreement between the quantum and classical calculations. The calculated maximum energy agrees with the classical estimate (15) for high impact velocities, $k_0\simeq 1$. For slower particles, maximum velocity is slightly above the estimate (15) for the attractive potential and below that estimate for the repulsive one. This is because of the Coulomb potential energy contribution at the moment of collision. For slow particles ($k_0=0.7$), one can also see a dramatic difference between the attractive and repulsive potentials in the number of energetic particles. It differs more than one order of magnitude while their average energy remains the same. A higher number of hot electrons for the scattering in the attractive potential is a clear indication of the effect of correlated collisions (Coulomb focusing).

As the incident electron energy increases, the difference between the scattering on the positive and negative ion charges decreases. For the incident velocity $k_0=2$, which is twice as big as the quiver velocity, the model of instantaneous collisions reproduces the quantum results with a good accuracy. This indicates that the importance of correlated collisions is limited to relatively small electron velocities, $k_0\lesssim v_0$.

In all considered runs, the overall electron energy gain is very small, more than ten times smaller than the initial energy and the ponderomotive potential. Therefore, the formation of the hot electron tail is accompanied by slowing down and trapping of some electrons. The total number of accelerated electrons is relatively small, about 10^{-3} for the present parameters and $k_0\lesssim 1$. For $k_0\gtrsim 1$, the number of accelerated electrons decreases with the particle energy. For $k_0=2$, the classical dynamical model predicts $\sim 3\times 10^{-4}$ particles with energy larger than $\frac{1}{2}k_0^2+3U_p=2.75$. This number is still more than ten times the theoretical estimate (4×10^{-5}) based on the model of instantaneous collision developed in Ref. 15. However, this difference decreases with both the initial particle velocity and the electric-field strength. This is a consequence of the fact that the Rutherford cross section is a decreasing function of the incident particle energy.

VI. DISCUSSION AND CONCLUSIONS

In this paper, we demonstrated for the first time the effect of correlated electron-ion collisions in the laser field by direct solutions to the time-dependent Schrödinger equation in three spatial dimensions. This effect leads to large energy gains for electrons with velocities smaller than the electron quiver velocity in the laser field. This effect is most important for the case of parallel launch, where the incident electron velocity is parallel to the electric field vector. In this case, the correlated collisions lead to the formation of a tail of energetic electrons (with energies above at least three ponderomotive potentials) and with an approximate power-law energy distribution. The mean and cutoff energies are both described rather well by the classical model without any specific modification of the Coulomb potential at small distances. However, the classical model slightly underestimates the number of accelerated electrons and their maximum energy, while we found very good agreement for the average hot electron energy.

The quantum calculations demonstrate a similarity between the process of above-threshold ionization of a neutral atom and the correlated collisions at small incident velocities, $k_0<v_0$. In both cases, a combination of the Coulomb and external electric fields makes the electron return to the scattering center and thereby a large amount of energy is transferred. We found that the electrons approaching the nuclei at the distances as small as one-hundredth of the atomic radius make an important contribution to the energy spectrum of scattered particles. Similarly to the ATI, the electrons are accelerated in the direction of the electric field polarization and, according to our calculations, the relative number of these electrons could be as large as 10^{-3}, which is much more than one would expect from the ordinary Coulomb collisions at small impact parameters. We also found that a significant number of electrons are recombining with the ions. Here, the difference between the classical treatment and the quantum calculations could be more significant. In particular, the classical calculations predict the electron trapped in the energy states below −0.5, which do not exist in the hydrogen atom.

Our analysis shows that the parameter range, where the

correlated collisions could be important, corresponds to relatively low laser intensities, long wavelengths, and small electron energies of the order of a few atomic units. However, this conclusion is limited to the electron scattering on a proton and to the XUV frequency range. The higher Z ions and the laser fields in the optical frequency range might offer new, yet unexplored, possibilities.

The effect of correlated collisions increases significantly the number of energetic particles, and that might have some important manifestations in applications. It might explain the anomalously high x-ray production[14] and enhanced ionization[23] in clusters at relatively low laser intensities. This effect can also result in the anomalously high laser absorption rates and generation of hot electron populations. A direct experimental verification of the effect of correlated electron-ion collisions would be an important step in the development of the understanding of laser-matter interaction physics.

ACKNOWLEDGMENTS

Allocation of CPU time and assistance with the computer facilities from the "Centre Informatique National de l'Enseignement Supérieur" (CINES, Montpellier, France) are acknowledged.

[1] J. Dawson and C. Oberman, Phys. Fluids **5**, 517 (1962).
[2] V. P. Silin, Sov. Phys. JETP **20**, 1510 (1965).
[3] F. V. Bunkin and M. V. Fedorov, Sov. Phys. JETP **22**, 844 (1966).
[4] F. V. Bunkin, A. E. Kazakov, and M. V. Fedorov, Sov. Phys. Usp. **15**, 416 (1972).
[5] N. M. Kroll and K. M. Watson, Phys. Rev. A **8**, 804 (1973).
[6] G. J. Pert, J. Phys. A **5**, 506 (1972); J. Phys. B **12**, 2755 (1979).
[7] C. D. Decker, W. B. Mori, J. M. Dawson, and Y. Katsouleas, Phys. Plasmas **1**, 4043 (1994).
[8] G. Shvets and N. J. Fish, Phys. Plasmas **4**, 428 (1997).
[9] P. Mulser, F. Cornolti, F. Bésuelle, and R. Schneider, Phys. Rev. E **63**, 016406 (2001).
[10] H.-J. Kull and L. Plagne, Phys. Plasmas **8**, 5244 (2001).
[11] L. Wiesenfeld, Phys. Lett. A **144**, 467 (1990).
[12] G. M. Fraiman, V. A. Mironov, and A. A. Balakin, Phys. Rev. Lett. **82**, 319 (1999); JETP **88**, 254 (1999); G. M. Fraiman, A. A. Balakin, and V. A. Mironov, Phys. Plasmas **8**, 2502 (2001).
[13] A. Brantov, W. Rozmus, R. Sydora, C. E. Capjack, V. Y. Bychenkov, and V. T. Tikhonchuk, Phys. Plasmas **10**, 3385 (2003).
[14] C. Deiss, N. Rohringer, J. Burgdörfer, E. Lamour, C. Pringent, J.-P. Rozet, and D. Vernhet, Phys. Rev. Lett. **96**, 013203 (2006).
[15] H.-J. Kull and V. T. Tikhonchuk, Phys. Plasmas **12**, 063301 (2005).
[16] P. B. Corkum, Phys. Rev. Lett. **71**, 1994 (1993).
[17] P. Lambropoulos, P. Maragakis, and J. Zhang, Phys. Rep. **305**, 203 (1998).
[18] H. Bachau, E. Cormier, P. Decleva, J. E. Hansen, and F. Martín, Rep. Prog. Phys. **64**, 1815 (2001).
[19] C. de Boor, *A Practical Guide to Splines* (Springer, New York, 1978).
[20] H.-J. Kull, J. Görlinger, and L. Plagne, Laser Phys. **10**, 151 (2000).
[21] V. Ayvazyan, N. Baboi, I. Bohnet *et al.*, Phys. Rev. Lett. **88**, 104802 (2002).
[22] B. Yang, K. J. Schafer, B. Walker, K. C. Kulander, P. Agostini, and L. F. DiMauro, Phys. Rev. Lett. **71**, 3770 (1993).
[23] R. Santra and C. H. Greene, Phys. Rev. Lett. **91**, 233401 (2003).